Performance of *N,O*-Carboxymethyl Chitosan as Corrosion and Scale Inhibitors in CO_2 Saturated Brine Solution

Muhamad Jalil Baari[1*], Bunbun Bundjali[2], and Deana Wahyuningrum[2]

[1]*Department of Chemistry, Universitas Sembilanbelas November Kolaka, Jl. Pemuda, Kolaka, 93511, Indonesia*

[2]*Department of Chemistry, Institut Teknologi Bandung, Jl. Ganesha No. 10, Bandung 40132, Indonesia*

** **Corresponding author:***

email: jalilbaari@gmail.com

Received: February 22, 2021
Accepted: April 7, 2021

DOI: 10.22146/ijc.64255

Abstract: *The presence of salts and dissolved gas like CO_2 that is carried with natural gas and crude oil along the pipeline is the main reason for corrosion and scale formation. These problems are usually resolved separately by corrosion inhibitors and scale inhibitors or acidification. Meanwhile, utilizing a compound to resolve both corrosion and scale formation has an advantage in the economic side and working time.* N,O-*carboxymethyl chitosan or* N,O-*CMCs is one of the chitosan's derivates. It is water-soluble and has different functional groups. Those properties support its capability as a complexing agent on corrosion and scale inhibitors. Synthesis of* N,O-*CMCs was carried out by chemical reactions between chitosan and chloroacetic acid under alkaline circumstances.* N,O-*CMCs product was characterized using FT-IR and* ^{1}*H-NMR spectroscopy. The inhibition efficiency was analyzed by electrochemical impedance spectroscopy (EIS) and potentiodynamic polarization techniques. The measurements showed that the highest efficiency of corrosion inhibition reached 63.54% when the concentration and temperature were 30 ppm and 35 °C, respectively.* N,O-*CMCs was classified as a mixed-type inhibitor. The adsorption mechanism of the inhibitor followed Langmuir adsorption isotherm. The static scale inhibition test informed that the optimum inhibition efficiency of* N,O-*CMCs reached 60.00%.*

Keywords: N,O-*carboxymethyl chitosan; corrosion inhibitor; carbon steel; scale inhibitor*

■ INTRODUCTION

Corrosion and scale formation are severe problems on pipelines of the petroleum industry. Those correspond to natural gas and crude oil transportation from the oil wells to the processing and storage stages through the pipeline containing corrosive substances such as water, chloride, minerals, and dissolved CO_2 [1-2]. Generally, carbon steel is a primary material for pipeline construction due to its good physical and mechanical properties [3]. Availability and lower price are the other reasons when uses this material [4]. However, carbon steel is rapidly corroded after contacting with corrosive environments.

Meanwhile, deposition of $CaCO_3$ on the inner surface of the pipeline will reduce the stream of fluids and triggers localized corrosion attacks (formed pitting corrosion) [5]. Consequently, pipeline leakage is unavoidable. The utilization of acid solutions can prevent or dissolve scale formation, but the aggressiveness of fluids also increases simultaneously, accelerating the pipeline failure [6]. Besides that, the accumulation of acid solution is very harmful to organisms around the contaminated area.

Corrosion and scale problems are usually treated separately by corrosion and scale inhibitors with different compounds [7-9]. However, the use of a compound that has double functions as the corrosion inhibitor and scale inhibitor is an advantage. Organic corrosion inhibitors have been widely used owing to cost-effective, practical means, and contain oxygen, nitrogen, phosphor, sulphur atoms that have π and lone pair electrons in their molecular structure to be

adsorbed on the metal surface by sticking on active sites [10-11]. Previous studies inform that corrosion inhibitors from polymeric compounds can be adsorbed strongly than monomer units or simple compounds [12-13]. On the other hand, scale inhibitors from polymer compounds are powerful complexing agents toward calcium and magnesium ions, good thermal stability, and better environmental compatibility [6,12]. A potential biopolymer as both corrosion and scale inhibitor is carboxymethyl chitosan (CMCs). It is a chitosan derivative that can be synthesized from the shell of crustaceans, for instance, shrimp, lobster, or crab. CMCs have different functional groups compared to chitosan so that it is easily dispersed into the aqueous solution and adsorbed onto a metal surface and $CaCO_3$ crystal surface [14]. The other characteristics of this polymer include biocompatible, biodegradable, low toxicity, antioxidant, and antibacterial [15-16].

CMCs are classified into several types according to the position of carboxymethyl groups in the glucosamine rings, including *N*-CMCs, *N,N*-CMCs, *O*-CMCs, and *N,O*-CMCs respectively [17]. Each type of CMCs is obtained through different synthesis processes [18]. *N,O*-CMCs is a type of carboxymethyl chitosan in which carboxymethyl groups are bound to amine groups on C-2 atoms and two hydroxyl groups on C-6 and C-3 atoms (Fig. 4). Previous studies had shown that carboxymethyl chitosan could be used as a corrosion inhibitor in several media [19-20]. However, there is no information about the natural source of chitosan, a specific type of CMCs, utilization of CO_2 in the corrosive medium, and its performance as a scale inhibitor. Therefore, this research aims to synthesize *N,O*-CMCs from shrimp shell waste and to study its performance as corrosion and scale inhibitors in the saturated CO_2 solution for metal protection. Adsorption isotherm and adsorption energy are also studied.

■ EXPERIMENTAL SECTION

Materials

Shrimp shell waste was obtained from Makassar, South Sulawesi. Chemicals were analytical grades consisting of sodium hydroxide, hydrogen chloride (37%), sodium chloride, potassium bromide, chloroacetic acid, absolute ethanol (99%), isopropanol, $MgCl_2{\cdot}6H_2O$, $CaCl_2{\cdot}2H_2O$, sodium bicarbonate, ethylene diamine tetraacetate dehydrate, potassium hydroxide, and calcium indicator. All chemicals were procured from Merck.

Instrumentation

The structure characterization of *N,O*-CMCs was conducted by proton nuclear magnetic resonance (^{1}H-NMR) Bruker Avance 500 MHz and Fourier transform infrared (FT-IR) ALPHA Bruker Spectrometers. The effectivity of corrosion inhibition was electrochemically analyzed by Voltalab PGZ 301 potentiostat with three electrodes configuration. All electrodes were immersed in NaCl (1.0%) solution with continuous sparging of CO_2. Composition of carbon steel as the testing metal were C (0.1%), S (0.03%), Mn (0.45%), P (0.025%), and balanced Fe [21].

Procedure

Preparation of chitin and chitosan

NaOH 3.5% (w/v) solution was mixed to shrimp shell powder in a ratio of 1:10 for 2 h at 68 °C for the deproteination stage. Then, demineralization was carried out by adding HCl 1 M solution to protein-free chitin in a ratio of 1:15 for 2 h at room temperature. After that, chitosan was synthesized by the triple deacetylation of chitin. In this stage, the mixture of chitin and NaOH 50% (w/v) solution was refluxed in a ratio of 1:15 for 3 h at 110 °C. The deacetylation degree (DD) of obtained chitosan was determined based on the baseline method from the IR spectra. It was calculated by Eq. (1) [22].

$$DD = 100 - \left(\frac{A_{1655}}{A_{3450}} \times \frac{100}{1.33} \right) \quad (1)$$

where A_{1655} and A_{3450} are vibrational absorbances of carbonyl in amides at 1655 cm^{-1} and amine groups at 3450 cm^{-1}, respectively. Factor 1.33 is a value from the ratio between A_{1655} and A_{3450} through a specific baseline. A viscometric method using the Ostwald viscometer was determined by the average molecular weight (AMW) of chitosan. Specific viscosity was measured by observing the time of flowing fluid with and without chitosan,

respectively, then determined the reduced viscosity and intrinsic viscosity ([η]) of each solution. Furthermore, the average molecular weight of the viscosity $\overline{M_v}$ was calculated by the Mark-Houwink formula like on Eq. (2) [23].

$$[\eta] = K.\overline{M_v}^{\alpha} \quad (2)$$

where value of $K = 1.4 \times 10^{-4}$ mL g^{-1} and $\alpha = 0.83$, $\overline{M_v}$ is the average molecular weight of viscosity.

Synthesis of N,O-CMCs

N,O-CMCs was synthesized by modification Zheng and partner method. NaOH (7.2 g) was dissolved in the mixture of 25 mL demineralized water and 50 mL isopropanol. Then, chitosan (4.0 g) was added to this mixture and reacted at room temperature for 1 h. Afterward, 5.0 g chloroacetic acid that had dissolved in 10 mL demineralized water-isopropanol solution at a ratio of 1:4 was slowly dropped to chitosan suspension. This solution was reacted for 4 h at 50 °C. Furthermore, the solution was acidified by adding HCl 2 M solution, neutralized by 80% of ethanol, washed with ethanol (95%), rinsed with concentrated ethanol, and dried inside of the oven at 65 °C for 24 h [24]. The structure elucidation of *N,O*-CMCs was conducted with ^{1}H-NMR and FT-IR Spectrometers. Modification of chitin to chitosan and *N,O*-CMCs is displayed in Fig. 1.

Performance analysis of corrosion inhibitor

Performance analysis of corrosion inhibitor was conducted by electrochemical impedance spectroscopy (EIS) and potentiodynamic polarization techniques. These experiments used potentiostat with a three-electrodes configuration. Carbon steel was used as a working electrode, platinum as an auxiliary electrode, and saturated calomel electrode (SCE) as a reference electrode. The working electrode was formed to a cylindrical rod (cross-section surface area of 1.13 cm^2) which was embedded in an epoxy resin. Before starting the analysis, the exposed surface of the working electrode was polished with 800, 1200, 2000 grit emery-papers on a Heidolph rotator, washed with demineralized water, and rinsed by ethanol. All electrodes were connected to a potentiostat. The flask was filled with 100 mL NaCl 1% solution and continued by fulfillment CO_2 gas throughout the experiment. The self-assembly of electrochemical measurements in this experiment is displayed in Fig. 2. For the EIS technique, temperature variations were 25, 35, 45, and 55 °C, respectively. The operating frequency was in the range of 10 kHz–100 mHz, and the variations of inhibitor concentration were 6, 12, 18, 24, and 30 ppm, respectively. Meanwhile, corrosion inhibition analysis by potentiodynamic polarization technique was carried out by taking a temperature that generates the highest inhibition efficiency from the EIS technique with several concentrations (18, 24, 30, and 36 ppm). Inhibition efficiency by EIS and potentiodynamic polarization techniques were calculated using Eq. (3) and Eq. (4) [25-26].

$$IE = \frac{Rp_{inh} - Rp}{Rp_{inh}} \times 100\% \quad (3)$$

$$IE = \frac{I_{corr\,o} - I_{corr\,inh}}{I_{corr\,o}} \times 100\% \quad (4)$$

where IE is inhibition efficiency of inhibitor (%), Rp_{inh} is polarization resistance with inhibitor (Ohm cm^2), Rp is polarization resistance without inhibitor (Ohm cm^2), $I_{corr\,o}$ and $I_{corr\,inh}$ (mA cm^{-2}) are corrosion current density of the system without and with inhibitor.

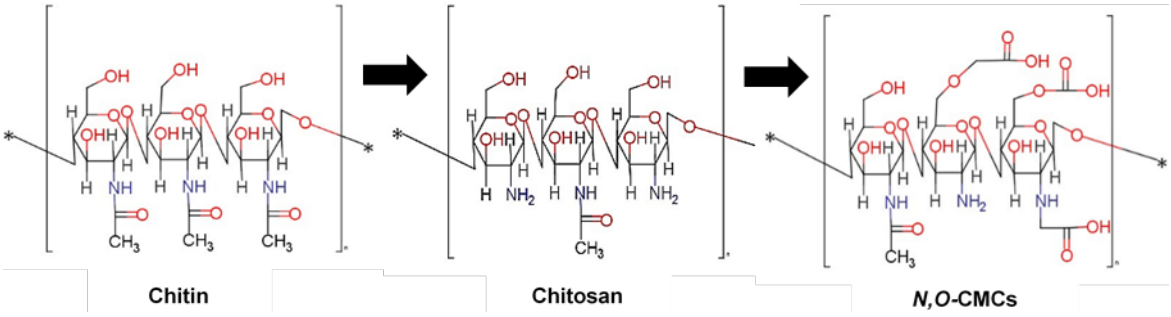

Fig 1. Modification chitin to chitosan and *N,O*-CMCs [15]

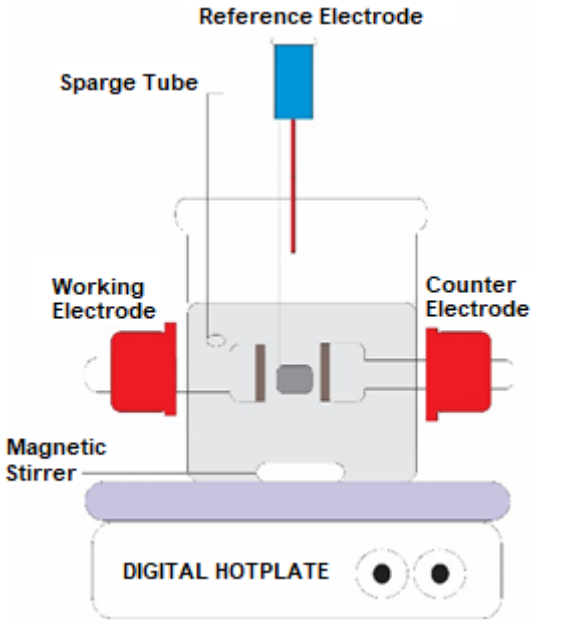

Fig 2. Self-assembly of electrochemical measurements

Study of adsorption isotherm

The surface coverage of the inhibitor (θ) on the metallic surface correlated to the efficiency of corrosion inhibition which is shown in Eq. (5) [27].

$$\theta = \frac{Rp_{inh} - Rp}{Rp_{inh}} \text{ or } \frac{IE(\%)}{100} \quad (5)$$

The adsorption process of *N,O*-CMCs on the metal surface was matched to various adsorption isotherms such as Langmuir, Freundlich, and Temkin isotherms. The adsorption type of inhibitor (physisorption, chemisorption, or physical-chemical adsorption) was determined by the value of the standard Gibbs free energy of adsorption (ΔG^{o}_{ads}) that is displayed in Eq. (6) [26-27].

$$\Delta G^{o}_{ads} = -RT\ln(55.55K_{ads}) \quad (6)$$

where R is the constant (8.314 J mol^{-1} K^{-1}), the value of 55.55 is water concentration in 1000 mL solution (mol L^{-1}), and T is the temperature (K).

Analysis of scale inhibition

This test followed NACE Standard TM0374-2001 about the Standard Test Method Laboratory Screening Test that based on the capability of scale inhibitors to restrain the precipitation of calcium carbonate in a solution. Initially, the mixture of 3.68 g, $MgCl_2{\cdot}6H_2O$, 12.15 g $CaCl_2{\cdot}2H_2O$, and 33.0 g NaCl was dissolved in demineralized water to attain 1.0 L calcium brine solution. Then, 1.0 L carbonic brine solution was obtained by dissolve 7.36 g $NaHCO_3$ and 33 g NaCl into demineralized water [28]. Both brine solutions were mixed into the vessels and were divided for the solution without the addition of inhibitors in various concentrations (6, 12, 18, 24, and 30 ppm). The solution was bubbled with CO_2 to remove O_2. Non-inhibitor solutions were specifically distinguished through heating at 71 °C for 24 h and without going through heating.

Meanwhile, all solutions with inhibitors were heated at 71 °C for 24 h. After cooling in the atmosphere, the next stage was to analyze residual Ca^{2+} concentration and scale inhibition efficiency by titration method with standard ethylene diamine tetraacetate dehydrate (EDTA) solution. This analysis was repeated two times to get accurate results.

■ RESULTS AND DISCUSSION

Isolation of Chitin, Synthesis of Chitosan and Their Characterizations

The deproteination step was intended to cut off atomic interactions, such as Van der Waals forces, covalent bonds, electrostatic forces, and hydrogen bonds among polymer chains of chitin with amino acids. The demineralization step can reduce mineral content on shrimp shells such as $CaCO_3$ and $Ca_3(PO_4)_2$ [23]. Functional group analysis of chitin is displayed on the IR spectra in Fig. 3. The spectra show peaks at wavenumber 3263 cm^{-1} and 3446 cm^{-1}, which relate to stretching vibrations of –OH in alcohol groups by intermolecular and intramolecular hydrogen bonds. Besides that, those peaks also correspond to the stretching vibrations of –NH in acetamide groups. The existence of C–H groups on alkane (–CH_3 and –CH_2) is displayed by absorption peaks in the wavenumber range 2891–2960 cm^{-1} from stretching vibrations in phase and out of phase. Whereas the C–H vibrations of the methine groups only have bending vibration at 1315 cm^{-1}. The presence of the C–O bond in the alkoxy group is confirmed by absorption peaks at wavenumber 1028–1112 cm^{-1}. The typical peak of chitin lies in the wavenumber 1655 cm^{-1} with a very high intensity derived from the carbonyl (C=O) stretching vibrations in the acetamide group.

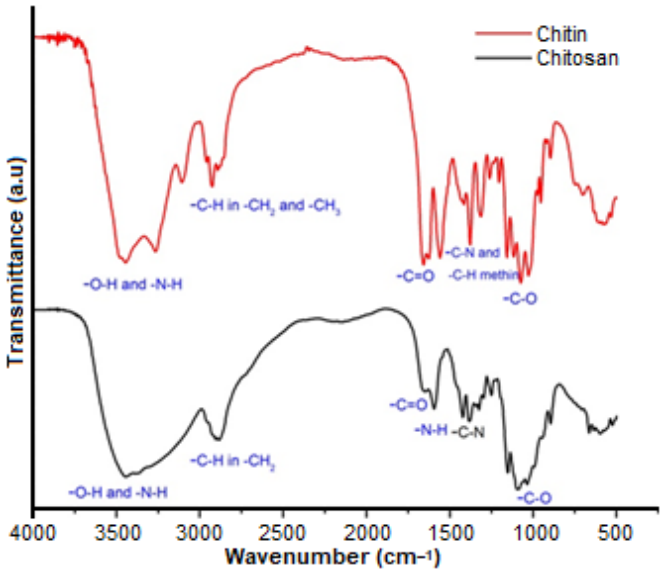

Fig 3. IR spectra of chitin and chitosan

The synthesis of chitosan from chitin was carried out by the deacetylation process. In this stage, chitin was hydrolyzed by a concentrated NaOH solution and high temperature to produce primary amine groups after releasing acetyl groups in glucosamide rings [29]. This stage was carried out three times to get optimization in the hydrolysis chitin. The IR spectra of chitosan are displayed in Fig. 3. Some absorption peaks are similar to the IR spectra of chitin. The differences lie in the reduced intensity of the vibrational peak of C=O from the acetyl group at 1655 cm^{-1} and the appearance of a peak at wavenumber 1596 cm^{-1} resulted from bending vibration of N–H bonds in primary amine groups [16].

Mass of chitin and chitosan after deproteination, demineralization, and deacetylation from 75 g shrimp shell powders, DD, and AMW of chitosan are shown in Table 1.

Table 1 displays that deacetylation of chitosan repeatedly can increase the degree of deacetylation until reaching 81.46%. This is followed by the decrease of molecular weight due to the change of acetyl groups to primary amines and accompanied by the possibility of breaking glycosidic bonds on the several polymer chains. The average molecular weight of chitosan from the first deacetylation cannot be determined by the viscometric method because there are still many acetyl groups in the polymer chains.

Synthesis and Characterization of *N,O*-Carboxymethyl Chitosan

The change of chitosan into carboxymethyl chitosan was intended to improve its solubility and surface-active property [30]. Improvements of these characters depend on the degree of substitution and the possibility of secondary reactions like cross-linking reactions during the synthesis process [31]. IR spectra of *N,O*-CMCs are shown in Fig. 4. The presence of –OH groups from carboxymethyl (–CH_2COOH) and alcohol groups on glucosamine rings (C-6 and C-3) is displayed by the extensive peak of about 3000–3450 cm^{-1}. A new peak at wavenumber 1739 cm^{-1} comes from the vibration of carbonyl bonds in the carboxyl groups [16,22]. Furthermore, the peak at wavenumber 1030 cm^{-1} due to stretching vibration of C–O from –CH_2–OH, which appeared on the chitosan spectra, becomes weaker. While stretching vibrations –C–O– from –CH–OH groups at 1070 cm^{-1} still clearly appear. This indicates carboxymethylation on the chitosan mostly in C-6 [32]. More significant steric obstacles of the –OH group in C-3 lead to fewer carboxymethylation in this site [33]. The

Table 1. Synthesis steps, product, and several characterization results such as percent yield, deacetylation degree (DD), and average molecular weight (AMW)

No	Stages	Product	Mass (g)	Percent yield (%)	DD (%)	AMW (amu)
1	Deproteination	Chitin + minerals	37.5	50.00	-	-
2	Demineralization	Chitin	14.7	39.20	-	
3	Deacetylation 1	Chitosan	10.8	73.47	52.23	u
4	Deacetylation 2	Chitosan	9.8	90.74	62.45	2.00×10^6
5	Deacetylation 3	Chitosan	7.8	79.59	81.46	1.36×10^6

u: cannot be determined because chitosan is not soluble in the used solvent

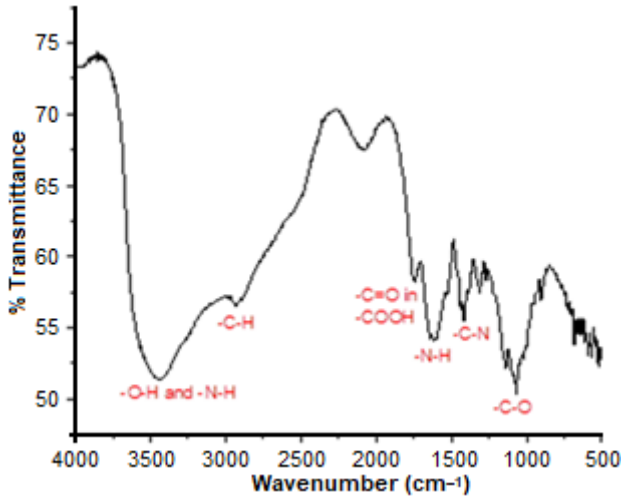

Fig 4. IR spectra of *N,O*-carboxymethyl chitosan (with KBr pellet)

peak intensity at 1383 cm^{-1} from the vibration C–N bond does not increase significantly to indicate that carboxymethyl groups are also not much bound to the amine groups [34]. Bending vibration of N–H bonds generates absorption peak at wavenumber 1596 cm^{-1} to indicate primary amines in the produced *N,O*-CMCs.

The type of protons composing *N,O*-CMCs were determined by ^{1}H-NMR spectroscopy. ^{1}H-NMR spectra in Fig. 5 show proton signals in *N,O*-CMCs compound. The signal intensity is low due to the poor solubility of *N,O*-CMCs in a small amount of D_2O. This corresponds to the lower degree of substitution of *N,O*-CMCs. More deshielding methylene protons from ^{1}H-NMR spectra are due to the environment adjacent to the electronegative groups, such as oxygen ether and oxygen carboxyl. Therefore, these protons have low electron density.

The presence of methyl protons in acetyl groups of *N,O*-CMCs is displayed by a signal at chemical shift 1.95 ppm. It explains that deacetylation processes to primary amines do not occur as a whole when converting chitin to chitosan [31]. Strong signals at 3.95 ppm and 3.97 ppm indicate that carboxymethylation mainly occurs in the hydroxyl groups at C-3 and C-6. Carboxymethylation on primary amines is shown by a signal at a chemical shift of 3.24 ppm [35]. Then, a powerful signal at 4.7 ppm comes from the solvent's undeuterated parts.

Analysis of Corrosion Inhibition

Fig. 6(a) and 6(b) represent a plot of inhibition efficiency (%) and polarization resistance (Ohm cm^2) as a function of *N,O*-CMCs concentration at several temperatures. The increment of polarization resistances describes that inhibitor molecules have covered active sites on the metal surface and form a protective layer on the metal-solution interface [36-37]. A low concentration of *N,O*-CMCs was found to have reduced the corrosion rate. *N,O*-CMCs has too large molecular size, which can be adsorbed and occupies a wider area on the carbon steel surface. Adsorption processes of polymeric inhibitor on metal surface in aqueous solution are via substitution reactions with water molecules [38]. There are many heteroatoms (oxygen and nitrogen) and π electrons of

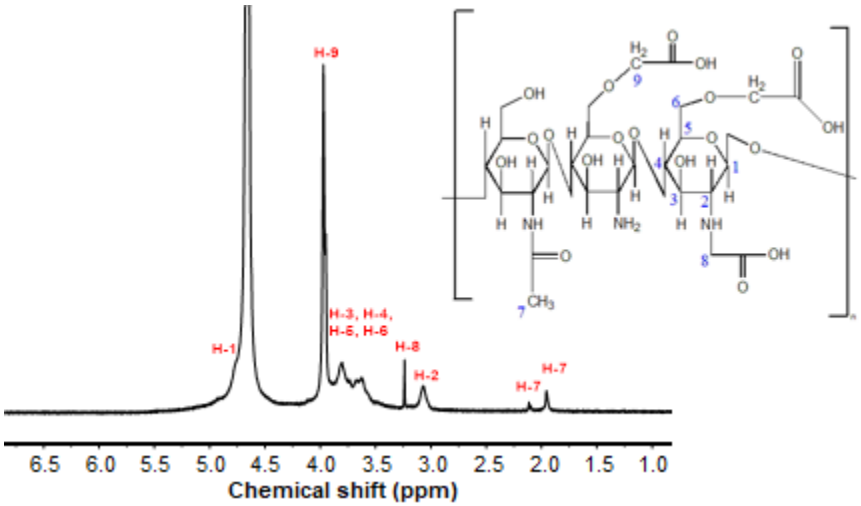

Fig 5. ^{1}H-NMR spectra of *N,O*-CMCs (in D_2O solvent)

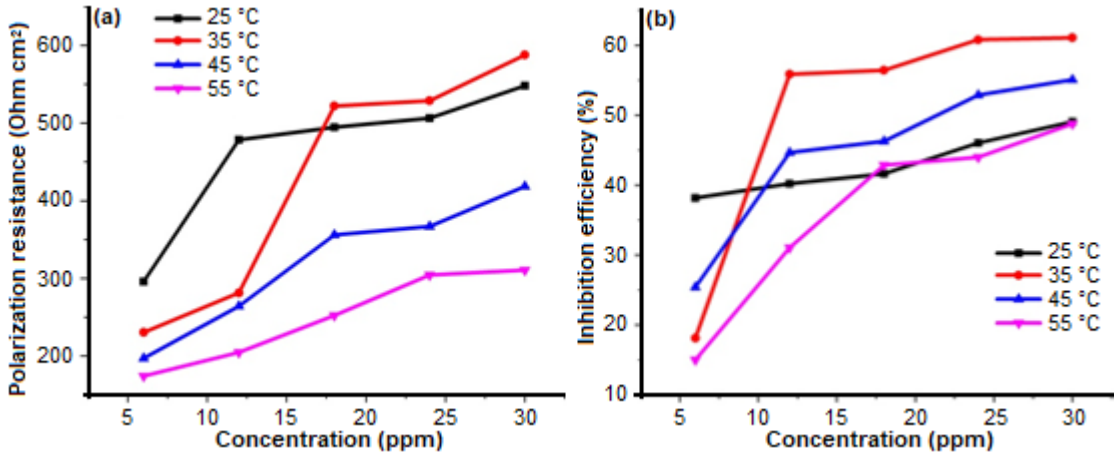

Fig 6. Plots of polarization resistance (a) and inhibition efficiency (b) by the presence of *N,O*-CMCs at various concentrations and temperatures

multiple bonds in *N,O*-CMCs molecular structure to make coordination bonding with ions or vacant *d*-orbitals of iron in the metal surface (chemisorption) [39-40].

Electrostatic and/or dipole-ion interactions can also occur among iron ions and/or iron atoms on the metal surface with carboxylate ions from *N,O*-CMCs compounds (physisorption). Besides that, there are electrostatic interactions between adsorbed chloride ions and positively charged inhibitor molecules from amine groups [41]. Bumby curves can be related to the difference in inhomogeneities and roughness of the working electrode surface during the analysis [42]. The formula of polarization resistance (R_p) is shown in Eq. (7).

$$R_p = Z_{re\,f\ min} - Z_{re\,f\ max} \quad (7)$$

where $Z_{re\,f\,max}$ is real impedance at a maximum frequency (Ohm cm^2), and $Z_{re\,f\,min}$ is actual impedance at a minimum frequency (Ohm cm^2). Values of the corrosion potentials (E_{corr}), solution resistance (R_s), polarization resistance (R_p), and inhibition efficiency (IE) are listed in Table 2. The highest efficiency was obtained at 35 °C when the inhibitor concentration was 30 ppm. This efficiency tends to be stable since the concentration continues to be increased. Then, it decreased again by increasing temperatures because higher temperatures can accelerate metal dissolution and diffusion processes of CO_3^{2-} and H^+ ions in solution to go to the active sites of metal [43]. Besides that, higher temperatures will desorb inhibitor molecules that are physically adsorbed from the metal-solution interface [44]. Structural decomposition and structural rearrangement may also occur [45-46]. However, protection to the metal surface from corrosion attack is still maintained.

The analysis of corrosion inhibition was also carried out by the potentiodynamic polarization technique. This method especially measures some electrochemical quantities such as corrosion current density and corrosion rate at 35 °C, which gives the highest efficiency from EIS.

The type of inhibitor (anodic or cathodic inhibitor) can be accurately determined by this technique from potential shifting trends on the linear polarization curves. The polarization curves for several concentrations of *N,O*-CMCs resulted from this method are shown in Fig. 7.

Corrosion potential values were obtained more positively after raising concentration, but these shifts were not greater than 85 mV. Therefore, *N,O*-CMCs is classified as a mixed inhibitor with a dominant character as an anodic inhibitor [47-48]. As a mixed inhibitor, *N,O*-CMCs can retard metal dissolution in the anodic site as well as reduce reaction in the cathodic site [49]. Table 3 displays the highest efficiency for the potentiodynamic polarization technique when the inhibitor's concentration is 30 ppm. These results have a good agreement with EIS result. The addition of *N,O*-CMCs up to 36 ppm even decreased inhibition efficiency. It can be explained that polymer molecules prefer parallelly adsorbed on the metal surface in a low

Table 2. Electrochemical parameters calculated by EIS technique in 1% NaCl solution

Temperature (°C)	Concentration (ppm)	E_{corr} (mV Vs SCE)	R_s (Ohm cm^2)	R_p (Ohm cm^2)	IE (%)
25	Blank	-710.8	16.71	295.7	-
	6	-716.1	14.22	478.4	38.19
	12	-682.1	13.89	494.7	40.22
	18	-673.9	14.92	506.5	41.62
	24	-671.4	14.28	548.1	46.05
	30	-682.9	13.36	580.7	49.08
35	Blank	-716.4	15.46	230.3	-
	6	-714.3	15.30	281.3	18.13
	12	-686.0	15.81	522.0	55.88
	18	-678.1	15.32	528.8	56.45
	24	-675.9	16.03	587.9	60.83
	30	-671.8	15.77	592.6	61.11
45	Blank	-721.6	14.68	197.0	-
	6	-715.2	11.37	264.1	25.40
	12	-687.5	11.36	356.0	44.66
	18	-687.0	11.85	366.8	46.29
	24	-686.4	11.23	418.4	52.91
	30	-686.0	11.54	438.7	55.09
55	Blank	-730.0	11.35	173.9	-
	6	-728.3	11.16	204.6	15.00
	12	-703.2	10.76	252.2	31.05
	18	-700.1	10.79	304.3	42.85
	24	-699.8	10.69	310.6	44.01
	30	-695.0	10.71	339.6	48.79

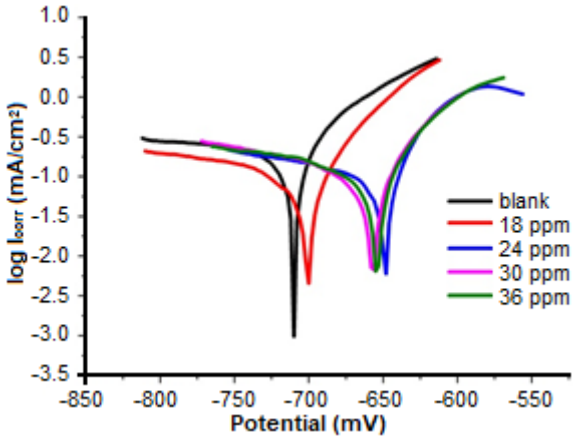

Fig 7. Polarization curves of *N,O*-CMCs at 35 °C

concentration to cover more active sites and accompanied by the expulsion of water molecules from the surface. These events continue until higher concentration that repulsive forces between inhibitor molecules were strong. In that condition, inhibitor molecules tend to be perpendicularly adsorbed on the metal surface to occupy a smaller surface area [50]. Another reason is the intermolecular attraction between the inhibitor molecules on the metal surface and the solution phase that can release adsorbed inhibitors from the carbon steel surface [8].

Study of Adsorption Isotherm and the Energy of Adsorption

Some types of adsorption isotherms (Langmuir, Freundlich, and Temkin isotherms) were matched to know the adsorption mechanism of *N,O*-CMCs on the working electrode surface. The type of adsorption isotherm and the values of parameters in adsorption energy are summarized in Table 4. Linear curves (Fig. 8) display adsorption of *N,O*-CMCs for some concentrations within the range of 25–45 °C on the carbon steel surface obtained from the formula of

Table 3. Electrochemical quantities calculated by potentiodynamic polarization technique with and without *N,O*-CMCs at 35 °C

Concentration (ppm)	Corrosion potential (mV)	Corrosion current density (mA/cm^2)	Corrosion rate (mmPY)	IE (%)
0	-710.0	0.2677	3.131	
18	-700.3	0.1135	1.327	57.60
24	-649.1	0.1068	1.249	60.10
30	-657.4	0.0976	1.141	63.54
36	-654.2	0.1691	1.977	36.83

Table 4. The types of adsorption isotherm, equilibrium constants of adsorption, and standard Gibbs free energies of adsorption (ΔG_{ads}) *N,O*-CMCs at range 25–55 °C

Temperature (°C)	Types of adsorption isotherm	K_{ads} (L/mol)	ΔG_{ads} (kJ/mol)	R_L
25	Langmuir	2.5×10^8	-57.90	0.559
35	Langmuir	5.0×10^8	-61.58	0.240
45	Langmuir	1.43×10^8	-60.26	0.689
55	Langmuir	5.0×10^7	-59.30	0.863

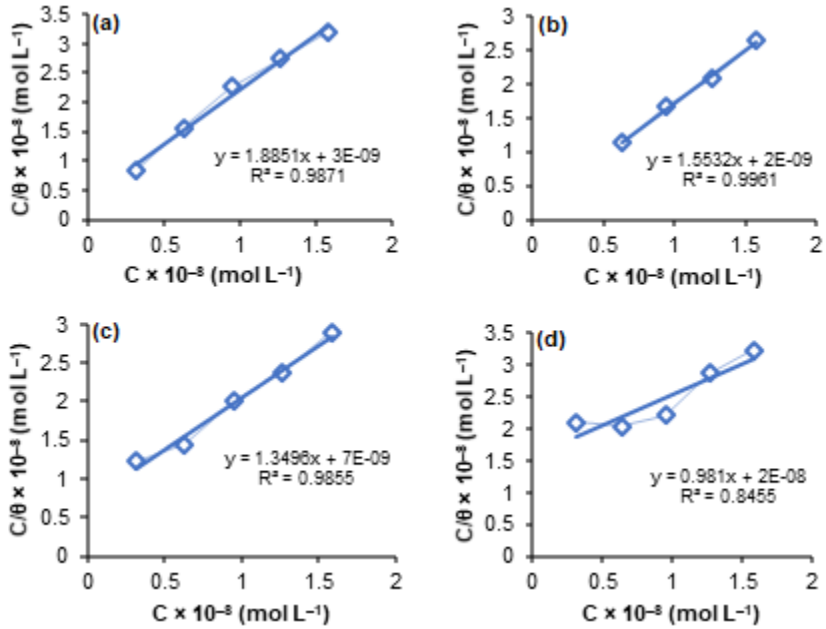

Fig 8. The linear relationship among several concentrations of *N,O*-CMCs (C_{inh}) and C_{inh}/θ, based on Langmuir adsorption isotherm in Eq. (8) at (a) 25, (b) 35, (c) 45, and (d) 55 °C, respectively

Langmuir isotherm adsorption in Eq. (8). It indicates that *N,O*-CMCs molecules have formed a monolayer on the metal surface without interaction between their neighbors [12].

$$\frac{C}{\theta} = \frac{1}{K_{ads}} + C \quad (8)$$

where C is the inhibitor's concentration (mol L^{-1}), θ is surface coverage, and K_{ads} is the equilibrium constant of adsorption-desorption (L mol^{-1}).

Whereas at 55 °C, the linear regression coefficient is relatively low ($R^2 < 0.900$), thus utilizing the first type of Langmuir isotherm is not fitted at this temperature. It was matched by another Langmuir equation and other isotherms like Freundlich and Temkin isotherm equations (Eq. (9)–(11)) to fix this discrepancy. Linear curves are displayed in Fig. 9.

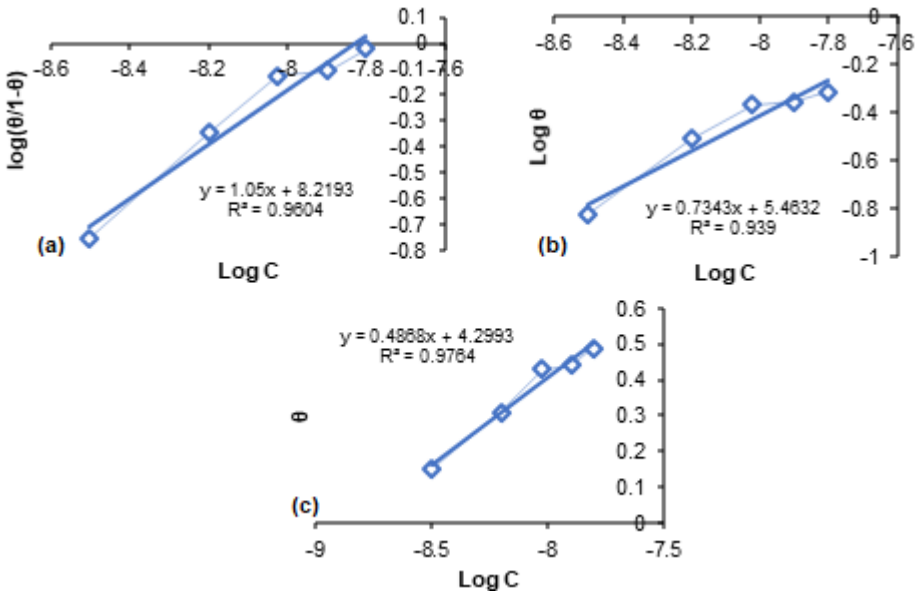

Fig 9. The linear relationship among several concentrations of *N,O*-CMCs and surface coverage (θ) based on (a) modified form of Langmuir adsorption isotherm, (b) Freundlich isotherm, and (c) Temkin isotherm at 55 °C

$$\log\left(\frac{\theta}{1-\theta}\right) = \log K_{ads} + \log C \quad (9)$$

$$\log\theta = \log K_{ads} + \frac{1}{n}\log C \quad (10)$$

$$\theta = \frac{1}{f}\log K_{ads} + \frac{1}{f}\log C \quad (11)$$

where 1/n relates to the adsorption intensity of *N,O*-CMCs onto the metallic surface, factor f is related to adsorbent-adsorbate interactions [51]. The dimensionless constant of the equilibrium parameter (R_L) is based on the utilization of the Langmuir equation to predict the efficiency of adsorption inhibitor on the metal surface. It was calculated by Eq.(12) [52].

$$R_L = \frac{1}{1+K_{ads}\cdot C} \quad (12)$$

The adsorption process is favorable occurred when the values of R_L are in the range 0 to 1, while $R_L > 1$, $R_L = 0$, and $R_L = 1$, indicate that adsorption is irreversible, unfavorable, and linear adsorption processes respectively [52].

The negative values from ΔG_{ads}, high values of K_{ads}, and the values of R_L parameter indicate the adsorption process of inhibitor molecules on to carbon steel surface is spontaneous and favorable [8,47]. Meanwhile, because ΔG_{ads} values are within the range -20 kJ mol^{-1} to -80 kJ mol^{-1}, therefore, adsorption mechanism of *N,O*-CMCs was a combination of physisorption and chemisorption [1].

Study of $CaCO_3$ Scale Inhibition

$CaCO_3$ crystals will be formed when the mixture of calcium and carbonate brine solutions were heated for 24 h. Calcium ion concentrations were obtained from consumed standard EDTA volume to reach the endpoint of the titration. The concentration of calcium ion and efficiency of scale inhibition was calculated using Eq. (13) and Eq. (14) [53].

$$\left[Ca^{2+}\right] = \frac{M_{EDTA}\cdot V_{EDTA}}{V_{system}} \quad (13)$$

$$IE = \frac{\left[Ca^{2+}\right]_{inh} - \left[Ca^{2+}\right]_{blank\ A}}{\left[Ca^{2+}\right]_{blank\ B} - \left[Ca^{2+}\right]_{blank\ A}} x100\% \quad (14)$$

where $[Ca^{2+}]_{blank\ A}$ and $[Ca^{2+}]_{blank\ B}$ are concentrations of calcium ion without inhibitor under heated/after precipitation and unheated/before precipitation respectively, M_{EDTA} is the molarity of EDTA, V_{EDTA} is the volume of EDTA, and $[Ca^{2+}]_{inh}$ is the concentration of calcium with the presence of inhibitor.

A lot of EDTA volumes that were consumed indicate higher content of calcium ions in the solution

Table 5. The average volume of EDTA solution that was needed for an equivalent point in titration, the concentration of calcium ions, and inhibition efficiency of *N,O*-CMCs against $CaCO_3$ scale in the various concentrations at 71 °C for 24 h

Solution	The average volume of EDTA (mL)	$[Ca^{2+}]$ (mol L^{-1})	IE (%)
0 ppm (unheated)	2.325	1.161×10^{-3}	-
0 ppm (heated)	1.700	8.490×10^{-4}	-
6 ppm	1.850	9.240×10^{-4}	24.04
12 ppm	1.925	9.620×10^{-4}	36.22
18 ppm	1.987	9.930×10^{-4}	46.15
24 ppm	2.033	1.015×10^{-3}	53.28
30 ppm	2.075	1.036×10^{-3}	60.00

phase. The action of inhibitor in solution could retard crystal nucleation and crystal growth of $CaCO_3$. Consequently, Ca^{2+} ions were longer dispersed in the solution phase, and the equilibrium concentrations of Ca^{2+} ions in the mixed brine solution increased than the solution without inhibitor. Kelvin equation in Eq. (15) explains the relationship between equilibrium concentration and the critical radius of $CaCO_3$ [14]. It was known that there is a decrease of critical radius from $CaCO_3$ crystal since the equilibrium concentration of ions increased.

$$\frac{\ln C}{C_0} = \frac{2\gamma M}{RT\rho r_c} \quad (15)$$

where C and C_0 are the equilibrium and initial concentrations of ion products (Ca^{2+}, CO_3^{2-}) and $CaCO_3$ respectively, γ is the surface tension of the crystal, M is the molar mass of the crystal, ρ is the density of $CaCO_3$, T is the testing temperature, R is the constant, and r_c is the critical radius of $CaCO_3$ crystal.

The capability of scale inhibition is attributed to hydroxyl, amide, and carboxyl groups, which are contained by inhibitor compound to improve chelating solubilization or complexing calcium ion, and maintain the dispersion effect to form $CaCO_3$ microparticles [14,54]. Table 5 reveals that the increment of *N,O*-CMCs concentration will increase scale inhibition efficiency until it reached 60.00% when the concentration is 30 ppm. It corresponds to the availability of more surface area and sorption sites to increase the metal adsorption capacity [6]. Further increase in concentrations may increase scale inhibition. However, this will decrease the corrosion inhibition effect. Ether groups in the carbon number 6 (C-6) from glucopyranose rings have the lone pair electrons that could also increase the adsorbed *N,O*-CMCs onto $CaCO_3$ crystal surface. Therefore, it has been good performance as a scale inhibitor at lower concentrations [54].

■ CONCLUSION

N,O-CMCs from shrimp shell waste had been synthesized by a chemical reaction between monochloro acetic acid and chitosan in base condition. Its structure was confirmed using FTIR and NMR characterizations. Analysis of corrosion inhibition efficiency toward carbon steel in the saturated CO_2 brine solution indicated that the increase of *N,O*-CMCs concentrations also increases inhibition efficiency. *N,O*-CMCs is effective enough as a green corrosion inhibitor at 35 °C when the concentration was 30 ppm. The optimum inhibition efficiency (*IE*) was 63.54%. However, this *IE* value is still lower than other green corrosion inhibitors like imidazole and its derivatives which *IE* value reaches 90%. *N,O*-CMCs is classified as a mixed-type inhibitor. Adsorption's processes obey Langmuir isotherm, which is dominated by chemical adsorption based on changes in the standard Gibbs free energy of adsorption. *N,O*-CMCs also acts as $CaCO_3$ scale inhibitors because they can improve the solubilization of calcium ions and the dispersion effect of $CaCO_3$ microparticles. The efficiency of scale inhibition reaches 60.0%. Further modifications on *N,O*-CMCs structure, may be considered to improve scale and corrosion inhibitions. Utilization of other

metals as a working electrode and other types of scale, such as $CaSO_4$ and $Ca_3(PO_4)_2$ are also helpful to know their interaction with *N,O*-CMCs.

■ AUTHOR CONTRIBUTIONS

All authors conducted the experiment and calculations. All authors wrote and revised the manuscript. All authors agreed to the final version of this manuscript.

■ REFERENCES

[1] Tawfik, S.M., and Negm, N.A., 2016, Synthesis, characterization and evaluation of some anionic surfactants with phosphate group as a biodegradable corrosion inhibitor for carbon steel in acidic solution, *J. Mol. Liq.*, 215, 185–196.

[2] Usman, B.J., and Ali, S.A., 2018, Carbon dioxide corrosion inhibitors: A review, *Arabian J. Sci. Eng.*, 43 (1), 1–22.

[3] Olivares-Xometl, O., López-Aguilar, C., Herrastí-González, P., Likhanova, N.V., Lijanova, I., Martínez-Palou, R., and Rivera-Márquez, J.A., 2014, Adsorption and corrosion inhibition performance by three new ionic liquids on API 5L X52 steel surface in acid media, *Ind. Eng. Chem. Res.*, 53 (23), 9534–9543.

[4] Salleh, N.I.H., and Abdullah, A., 2019, Corrosion inhibition of carbon steel using palm oil leaves extract, *Indones. J. Chem.*, 19 (3), 747–752.

[5] Kamal, M.S., Hussein, I., Mahmoud, M., Sultan, A.S., and Saad, M.A.S., 2018, Oilfield scale formation and chemical removal: A review, *J. Pet. Sci. Eng.*, 171, 127–139.

[6] Younes, A.A., El-Maghrabi, H.H., and Ali, H.R., 2017, Novel polyacrylamide-based solid scale inhibitor, *J. Hazard. Mater.*, 334, 1–9.

[7] El-Haddad, M.A.M., Radwan, A.B., Sliem, M.H., Hassan, W.M.I., and Abdullah, A.M., 2019, Highly efficient eco-friendly corrosion inhibitor for mild steel in 5 M HCl at elevated temperatures: Experimental & molecular dynamics study, *Sci. Rep.*, 9 (1), 3695.

[8] Baari, M.J., Bundjali, B., and Wahyuningrum, D., 2020, Synthesis of oligosuccinimide and evaluation of its corrosion inhibition performance on carbon steel in CO_2-saturated 1% NaCl solution, *J. Math. Fundam. Sci.*, 52 (2), 202–221.

[9] Li, C., Zhang, C., and Zhang, W., 2019, The inhibition effect mechanisms of four scale inhibitors on the formation and crystal growth of $CaCO_3$ in solution, *Sci. Rep.*, 9 (1), 13366.

[10] Raja, P.B., Qureshi, A.K., Rahim, A.A., Osman, H., and Awang, K., 2013, *Neolamarckia cadamba* alkaloids as eco-friendly corrosion inhibitors for mild steel in 1 M HCl media, *Corros. Sci.*, 69, 292–301.

[11] Saraswat, V., Yadav, M., and Obot, I.B., 2020, Investigations on eco-friendly corrosion inhibitors for mild steel in acid environment: Electrochemical, DFT and Monte Carlo Simulation approach, *Colloids Surf., A*, 599, 124881.

[12] Lv, J., Fu, L., Zeng, B., Tang, M., and Li, J., 2019, Synthesis and acidizing corrosion inhibition performance of N-doped carbon quantum dots, *Russ. J. Appl. Chem.*, 92 (6), 848–856.

[13] Biswas, A., Pal, S., and Udayabhanu, G., 2015, Experimental and theoretical studies of xanthan gum and its graft co-polymer as corrosion inhibitor for mild steel in 15% HCl, *Appl. Surf. Sci.*, 353, 173–183.

[14] Huang, H., Yao, Q., Jiao, Q., Liu, B., and Chen, H., 2019, Polyepoxysuccinic acid with hyper-branched structure as an environmentally friendly scale inhibitor and its scale inhibition mechanism, *J. Saudi Chem. Soc.*, 23 (1), 61–74.

[15] Mourya, V.K., Inamdar, N.N., and Tiwari, A., 2010, Carboxymethyl chitosan and its applications, *Adv. Mater. Lett.*, 1 (1), 11–33.

[16] Macedo, R.G.M.A., Marques, N.N., Paulucci, L.C.S., Cunha, J.V.M., Villetti, M.A., Castro, B.B., and Balaban, R.C., 2019, Water-soluble carboxymethylchitosan as green scale inhibitor in oil wells, *Carbohydr. Polym.*, 215, 137–142.

[17] Shariatinia, Z., 2018, Carboxymethyl chitosan: Properties and biomedical applications, *Int. J. Biol. Macromol.*, 120, 1406–1419.

[18] Upadhyaya, L., Singh, J., Agarwal, V., and Tewari, R.P., 2013, Biomedical applications of carboxymethyl chitosans, *Carbohydr. Polym.*, 91 (1), 452–466.

[19] Darmokoesoemo, H., Suyanto, S., Anggara, L.S., Amenaghawon, A.N., and Kusuma, H.S., 2018, Application of carboxymethyl chitosan-benzaldehyde as anticorrosion agent on steel, *Int. J. Chem. Eng.*, 2018, 4397867.

[20] Sun, H., Wang, H., Wang, H., and Yan, Q., 2018, Enhanced removal of heavy metals from electroplating wastewater through electrocoagulation using carboxymethyl chitosan as corrosion inhibitor for steel anode, *Environ. Sci. Water Res. Technol.*, 4 (8), 1105–1113.

[21] Bundjali, B., Surdia, N.M., Liang, O.B., and Ariwahjoedi, B., 2006, Pelarutan besi selektif pada korosi baja karbon dalam larutan buffer asetat, natrium bikarbonat - CO_2 jenuh, *J. Math. Fundam. Sci.*, 38 (2), 149–161.

[22] Domszy, J.G., and Roberts, G.A.F., 1985, Evaluation of infrared spectroscopic techniques for analysing chitosan, *Makromol. Chem.*, 186 (8), 1671–1677.

[23] Roberts, G.A.F., 1992, *Chitin Chemistry*, 1st Ed., Macmillan, London.

[24] Zheng, X., Zhang, H., She, Y., and Pu, J., 2014, Composite films of N,O-carboxymethyl chitosan and bamboo fiber, *J. Appl. Polym. Sci.*, 131 (3), 1–6.

[25] Qiang, Y., Fu, S., Zhang, S., Chen, S., and Zou, X., 2018, Designing and fabricating of single and double alkyl-chain indazole derivatives self-assembled monolayer for corrosion inhibition of copper, *Corros. Sci.*, 140, 111–121.

[26] Chaudhari, L.P., and Patel, S.N., 2019, Corrosion inhibition study of expired acetazolamide on mild steel in dilute hydrochloric acid solution, *J. Bio-Tribo-Corros.*, 5 (1), 1–13.

[27] Dagdag, O., Safi, Z., Erramli, H., Cherkaoui, O., Wazzan, N., Guo, L., Verma, C., Ebenso, E.E., and El Harfi, A., 2019, adsorption and anticorrosive behavior of aromatic epoxy monomers on carbon steel corrosion in acidic solution: Computational studies and sustained experimental studies, *RSC Adv.*, 9 (26), 14782–14796.

[28] NACE International, 2001, *Standard Test Method Laboratory Screening Tests to Determine the Ability of Scale Inhibitors to Prevent the Precipitation of Calcium Sulfate and Calcium Carbonate from Solution (for Oil and Gas Production Systems)*, NACE International, Houston, Texas.

[29] Jitareerat, P., Paumchai, S., Kanlayanarat, S., and Sangchote, S., 2007, Effect of chitosan on ripening, enzymatic activity, and disease development in mango (*Mangifera indica*) fruit, *N. Z. J. Crop Hortic. Sci.*, 35 (2), 211–218.

[30] Alsabagh, A.M., Elsabee, M.Z., Moustafa, Y.M., Elfky, A., and Morsi, R.E., 2014, Corrosion inhibition efficiency of some hydrophobically modified chitosan surfactants in relation to their surface active properties, *Egypt. J. Pet.*, 23 (4), 349–359.

[31] le Dung, P., Milas, M., Rinaudo, M., and Desbrières, J., 1994, Water soluble derivatives obtained by controlled chemical modifications of chitosan, *Carbohydr. Polym.*, 24 (3), 209–214.

[32] Larkin, P., 2011, *Infrared and Raman Spectroscopy Principles and Spectral Interpretation*, 1st Ed., Elsevier, Oxford, UK.

[33] Kim, C.H., Kim, S.Y., and Choi, K.S., 1997, synthesis and antibacterial activity of water-soluble chitin derivatives, *Polym. Adv. Technol.*, 8 (5), 319–325.

[34] Kong, X., 2012, Simultaneous determination of degree of deacetylation, degree of substitution and distribution fraction of –COONa in carboxymethyl chitosan by potentiometric titration, *Carbohydr. Polym.*, 88 (1), 336–341.

[35] Muzzarelli, R.A.A., Ilari, P., and Petrarulo, M., 1994, solubility and structure of N-carboxymethyl chitosan, *Int. J. Biol. Macromol.*, 16 (4), 177–180.

[36] Arjomandi, J., Moghanni-Bavil-Olyaei, H., Parvin, M.H., Lee, J.Y., Ko, K.C., Joshaghani, M., and Hamidian, K., 2018, Inhibition of corrosion of aluminum in alkaline solution by a novel azo-Schiff base: Experiment and theory, *J. Alloys Compd.*, 746, 185–193.

[37] Verma, C., Quraishi, M.A., and Singh, A., 2016, 5-Substituted 1H-tetrazoles as effective corrosion inhibitors for mild steel in 1 M hydrochloric acid, *J. Taibah Univ. Sci.*, 10 (5), 718–733.

[38] Kasshanna, S., and Rostron, P., 2017, Novel synthesis and characterization of vegetable oil

derived corrosion inhibitors, *J. Mater. Environ. Sci.*, 8 (12), 4292–4300.

[39] Douadi, T., Hamani, H., Daoud, D., Al-Noaimi, M., and Chafaa, S., 2017, Effect of temperature and hydrodynamic conditions on corrosion inhibition of an azomethine compounds for mild steel in 1 M HCl solution, *J. Taiwan Inst. Chem. Eng.*, 71, 388–404.

[40] El Faydy, M., Touir, R., Ebn Touhami, M., Zarrouk, A., Jama, C., Lakhrissi, B., Olasunkanmi, L.O., Ebenso, E.E., and Bentiss, F., 2018, Corrosion inhibition performance of newly synthesized 5-alkoxymethyl-8-hydroxyquinoline derivatives for carbon steel in 1 M HCl solution: Experimental, DFT and Monte Carlo simulation studies, *Phys. Chem. Chem. Phys.*, 20 (30), 20167–20187.

[41] Deng, S., Li, X., and Xie, X., 2014, Hydroxymethyl urea and 1,3-bis(hydroxymethyl) urea as corrosion inhibitors for steel in HCl solution, *Corros. Sci.*, 80, 276–289.

[42] Bentiss, F., Lebrini, M., and Lagrenée, M., 2005, Thermodynamic characterization of metal dissolution and inhibitor adsorption processes in mild steel/2,5-bis(n-thienyl)-1,3,4-thiadiazoles/hydrochloric acid system, *Corros. Sci.*, 47 (12), 2915–2931.

[43] Kahyarian, A., and Nesic, S., 2019, A new narrative for CO_2 corrosion of mild steel, *J. Electrochem. Soc.*, 166 (11), C3048–C3063.

[44] Chakravarthy, M.P., and Mohana, K.N., 2014, Adsorption and corrosion inhibition characteristics of some nicotinamide derivatives on mild steel in hydrochloric acid solution, *Int. Scholarly Res. Not.,* 2014, 687276.

[45] Barmatov, E., Hughes, T., and Nagl, M., 2015, Efficiency of film-forming corrosion inhibitors in strong hydrochloric acid under laminar and turbulent flow conditions, *Corros. Sci.*, 92, 85–94.

[46] Nešić, S., 2007, Key issues related to modelling of internal corrosion of oil and gas pipelines - A review, *Corros. Sci.*, 49 (12), 4308–4338.

[47] Verma, C., Singh, P., and Quraishi, M.A., 2016, A thermodynamical, electrochemical and surface investigation of Bis (indolyl) methanes as green corrosion inhibitors for mild steel in 1 M hydrochloric acid solution, *J. Assoc. Arab Univ. Basic Appl. Sci.*, 21, 24–30.

[48] Anejjar, A., Salghi, R., Zarrouk, A., Benali, O., Zarrok, H., Hammouti, B., and Ebenso, E.E., 2014, Inhibition of carbon steel corrosion in 1 M HCl medium by potassium thiocyanate, *J. Assoc. Arab Univ. Basic Appl. Sci.*, 15 (1), 21–27.

[49] Kaskah, S.E., Pfeiffer, M., Klock, H., Bergen, H., Ehrenhaft, G., Ferreira, P., Gollnick, J., and Fischer, C.B., 2017, Surface protection of low carbon steel with N-acyl sarcosine derivatives as green corrosion inhibitors, *Surf. Interfaces*, 9, 70–78.

[50] Wang, B., Du, M., Zhang, J., and Gao, C.J., 2011, Electrochemical and surface analysis studies on corrosion inhibition of Q235 steel by imidazoline derivative against CO_2 corrosion, *Corros. Sci.*, 53 (1), 353–361.

[51] Saadi, R., Saadi, Z., Fazaeli, R., and Fard, N.E., 2015, Monolayer and multilayer adsorption isotherm models for sorption from aqueous media, *Korean J. Chem. Eng.*, 32 (5), 787–799.

[52] Ayawei, N., Angaye, S., Wankasi, D., and Dikio, E.D., 2015, Synthesis, characterization and application of Mg/Al layered double hydroxide for the degradation of Congo Red in aqueous solution, *Open J. Phys. Chem.*, 5 (3), 56–70.

[53] Huang, H., Yao, Q., Liu, B., Shan, N., and Chen, H., 2017, Synthesis and characterization of scale and corrosion inhibitors with hyper-branched structure and the mechanism, *New J. Chem.*, 41 (20), 12205–12217.

[54] Feng, J., Gao, L., Wen, R., Deng, Y., Wu, X., and Deng, S., 2014, Fluorescent polyaspartic acid with an enhanced inhibition performance against calcium phosphate, *Desalination*, 345, 72–76.